Directional element for faulty feeder identification of high-resistance fault in high-surety power supply systems

Rouhani, Roja; Sadeghkhani, Iman; Guerrero, Josep M.

Published in:
IET Generation, Transmission and Distribution

DOI (link to publication from Publisher):
10.1049/gtd2.12006

Publication date:
2021

Document Version
Publisher's PDF, also known as Version of record

Received: 13 March 2020 | Revised: 1 September 2020 | Accepted: 18 September 2020

IET Generation, Transmission & Distribution

DOI: 10.1049/gtd2.12006

The Institution of Engineering and Technology WILEY

ORIGINAL RESEARCH PAPER

Directional element for faulty feeder identification of high-resistance fault in high-surety power supply systems

Roja Rouhani[1] | **Iman Sadeghkhani**[1] | **Josep M. Guerrero**[2]

[1] Department of Electrical Engineering, Najafabad Branch, Islamic Azad University, Najafabad, Iran

[2] Institute of Energy Technology, Aalborg University, Aalborg, Denmark

Correspondence
Iman Sadeghkhani, Department of Electrical Engineering, Najafabad Branch, Islamic Azad University, Najafabad 85141-43131, Iran.
Email: sadeghkhani@pel.iaun.ac.ir

Abstract

The high-surety power supply systems are gaining great attention to enhance the reliability of uninterruptable power supplies. A high-resistance fault along a high-surety power supply feeder results in a low fault current, making the conventional high-surety power supply protection strategy ineffective. To address this problem, this paper develops a directional fault protection strategy for high-resistance fault detection and faulty feeder identification. Using the intelligent electronic device, the feeder current is sampled and normalised. Then, the fault-imposed component of the current signal is calculated. This component is added to the input of the forced Helmholtz oscillator to increase the sensitivity of the proposed protection scheme for the detection of high-resistance faults. The output of the forced Helmholtz oscillator equation is adopted as the fault detection criterion because it is infinity for reverse faults while it is lower than 1 for forward faults, facilitating the fault detection. The developed strategy is local and can detect and classify both pole-to-ground and pole-to-pole high-resistance faults. Also, it is effective for both unidirectional and bidirectional converters. The merits of the proposed protection strategy are demonstrated through several fault scenarios using a ±375 V high-surety power supply system.

1 | INTRODUCTION

1.1 | Motivation

Critical loads such as hospitals, banks, and internet data centres require continuous and high-quality power during normal and faulty conditions [1, 2]. To this end, uninterruptable power supply (UPS) systems have been used for many years to make sure of continuous energy supply. To enhance the reliability of UPS systems, the concept of high-surety power supply (HSPS), also know as super UPS, has been recently introduced. An HSPS system is formed by several energy source and energy storage units such as photovoltaic (PV), battery, gas turbine, and super capacitor [3–6]. Certain attributes such as no harmonic and reactive power problems, no need for frequency control and complicated synchronisation, and low stages of power conversion make the DC network a proper selection for implementing the HSPS systems [7–10]. An HSPS system can operate in both grid-connected and islanded modes to ensure the continuous energy supply.

The lack of effective protection is one of the main barriers to the deployment of super UPS systems, jeopardising their offered resilience. Both pole-to-ground (PG) and pole-to-pole (PP) faults may occur in an HSPS system, by a pole coming in contact with the ground and another pole, respectively. DC nature of super UPS system makes its protection more challenging due to the following specific features: (i) in a DC network, there is no zero-crossing point in fault current, (ii) the capacitor discharge highly increases the magnitude and rate of change of fault current, (iii) the lines of DC networks are usually short, making the faulty feeder identification difficult.

1.2 | Literature review

Due to the need for high levels of reliability, speed, and selectivity, usually, the protection strategies proposed for DC microgrids are not effective in an HSPS system as follows. The current derivative-based protection schemes proposed in [11, 12] are susceptible to noise. The overcurrent protection

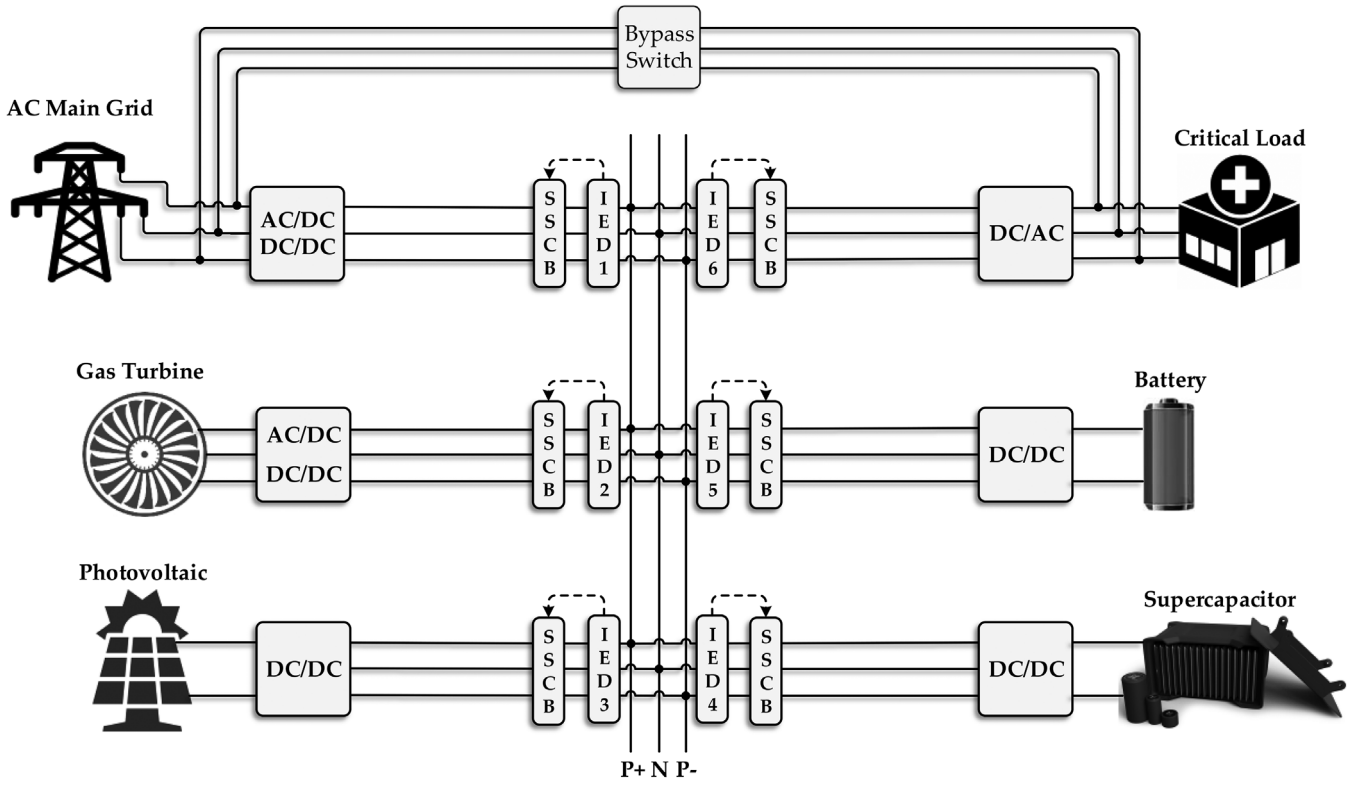

FIGURE 1 Study HSPS system

strategies proposed in [13, 14] cannot provide proper selectivity or require extra devices. The distance protection schemes proposed in [15, 16] suffer from low operating speed. The directional protection schemes proposed in [17–22] and differential protection methods proposed in [23–26] as the communication strategies increase selectivity; however, dependence on communication infrastructure decreases their reliability, making them improper for a high reliable power supply. To address these shortcomings, only one HSPS protection scheme is proposed; Li et al. [2] present a local current direction-based protection strategy for the HSPS systems. However, the conventional HSPS protection suffers from two problems: (1) it does not consider the dynamics of primary energy sources of HSPS system and (2) in the case of a high-resistance fault, the current direction does not change and consequently the current direction-based protection strategy fails.

1.3 | Aims and contributions

To address these problems, this paper proposes a protection scheme for the detection of high-resistance faults in super UPS systems. In the proposed local protection scheme that is a supplementary protection for the conventional HSPS protection, the current of each feeder is sampled using an intelligent electronic device (IED). Then, the fault-imposed component of the current is calculated to detect the direction change of high-resistance fault current. To increase the sensitivity of the proposed method, this component is added to the input of the forced Helmholtz oscillator (FHO). The advantage of the proposed directional protection scheme is that the FHO state variable is infinity for the faulty feeder while it has a finite value for the healthy one. Specifically, the contributions of this paper with respect to [2] are as follows:

- It considers the dynamics of primary energy sources of the HSPS system;
- It is effective for high-resistance faults; and
- It classifies the fault condition.

1.4 | Paper organisation

The rest of the paper is organised as follows. Section 2 describes the dynamic model, control system, and conventional protection scheme of the study HSPS system. The proposed two-stage protection strategy is developed in Section 3. Section 4 is dedicated to assessing the performance of the developed scheme. Finally, Section 5 concludes the paper.

2 | STUDY HSPS SYSTEM

Figure 1 shows the single diagram of the study HSPS system that is the extended version of the test system of [2]. It is a bipolar (three-wire) network with the TN-S earthing system

where the midpoint of the converter is connected to the ground. The operating voltage of the study HSPS is ±375 V. The resistance and inductance of the HSPS feeders are 4.8 mΩ and 3.8 μH, respectively. A 100 kW voltage-sourced inverter (VSI) is employed as the interface between the HSPS system and the main AC grid. The study HSPS system consists of five distributed energy resource (DER) units including gas turbine, energy storage system, PV array, supercapacitor, and fuel cell. The critical load is a three-phase, 220 V, 60 Hz, 230 kW, and 150 kVAr load that is interfaced with the HSPS system using a VSI. Also, a bypass switch is employed to directly connect the critical load to the AC main grid in the critical conditions.

2.1 | Dynamic modelling

The main grid is a 25 kV distribution system that is fed by a 120 kV transmission network with 2500 MVA short-circuit capacity. The distribution system is connected to the interface converter using a 100 kW, 25 kV/220 V Δ/Yg transformer. The interface converter is a three-phase three-level VSI, consisting of insulated gate bipolar transistor (IGBT) switches and antiparallel diodes. The AC side resistance, inductance, and capacitance of VSI are 0.0019 Ω, 250 μH, and 55 μF, respectively, while each capacitor of DC side of VSI is 12 mF. The PV system includes a 5×66 array (66 parallel strings with five modules in series in each string), consisting of 305.2 W SunPower modules. The open-circuit voltage, short-circuit current, maximum power point voltage, and maximum power point current are 64.2 V, 5.96 A, 54.7 V, and 5.58 A, respectively. The PV cells are mono-crystalline with the single diode model [14]. The adopted battery type is lithium-ion with the discharge and charge models. The supercapacitor is modelled using the Stern equation by considering the self-discharge phenomenon. The gas turbine is equipped with the IEEE type 1 excitation system. The PV array and fuel cell are interfaced to the HSPS system using the DC–DC boost converters, while the interfaces of the battery and supercapacitor are the bidirectional DC–DC converters. The generated AC electricity of the synchronous generator of the gas turbine is converted to DC using a rectifier; then, a buck converter is used to interface this generation system to the HSPS system.

2.2 | Control system

The control system of grid VSI is a two-loop control system. The objective of the external control loop is the regulation of DC link voltage while the inner control loop regulates the grid current real and reactive components. According to [2], each DER unit can operate in both voltage and current control modes. The control system of the DC–DC converters of DERs is shown in Figure 2. It consists of two control loops. The outer loop regulates the converter output voltage where the

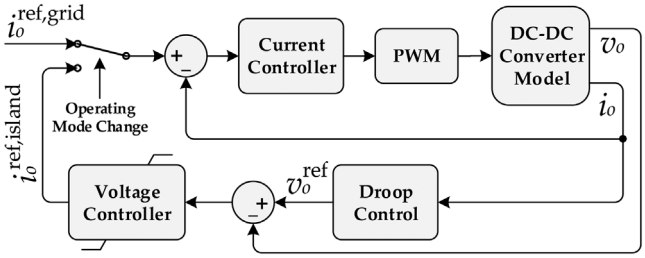

FIGURE 2 Basic structure of DC–DC converter control

reference voltage v_o^{ref} can be a predefined fixed value or can be calculated by a control scheme such as the droop control. The proportional-integral (PI) controller of the outer loop generates the reference signal for current control loop i_o^{ref}. The switching signals of the converter are generated using the pulse-width modulation (PWM) technique by the output of the PI controller of the inner loop. In the normal operating condition that the HSPS is in the grid-connected mode, the main grid regulates the HSPS voltage and the voltage control loop is deactivated in all DER units. In this case, i_o^{ref} is a predefined value or it is determined by the HSPS control centre. When a disturbance occurs in the main grid and the HSPS is in the islanded mode, one of the DER units goes to voltage control mode to stabilise the network voltage while others remain in the current control mode.

2.3 | Conventional current-based directional protection scheme

The basic principle of the directional protection proposed in [2] is the change of current direction in the case of a fault. In that method, the current is measured at the beginning of each feeder with a positive sign for the injected current to the HSPS system. When a fault occurs in one feeder, the main grid and DER units of other feeders contribute in fault current; thus, their current directions do not change and are positive, while for the faulty feeder, the current direction at the beginning of the feeder changes and is negative. There are two thresholds: one for negative currents and one for positive currents where the latter threshold is greater than the former one. If the measured current is negative and greater than the negative threshold, the feeder is faulty and is isolated from the HSPS system. If the primary protection fails, the fault persists in the HSPS system and the positive fault current of healthy feeders exceeds the latter threshold. In this condition, these feeders are isolated from the HSPS system as backup protection. Similarly, when a fault occurs in the main feeder of the HSPS system, all measured fault currents are positive and exceed the second threshold; thus all units are isolated from the HSPS system. In both cases of primary protection failure and main bus fault, the load voltage drops and the load module activates the bypass switch; in this condition, the load is directly supplied by the main grid.

3 | PROPOSED DIRECTIONAL PROTECTION STRATEGY

The main drawback of the conventional protection system of HSPS is its inability to detecting high-resistance faults. When a high resistance fault occurs, the fault current is low and it cannot change the current direction in the faulty feeder. Thus, the fault persists in the HSPS system. Also, the conventional protection lacks a fault classification scheme. The remainder of this section is dedicated to developing a two-stage protection strategy of the HSPS system for addressing these problems.

3.1 | First stage: Fault-imposed current

In the proposed local protection strategy, the injected current of each feeder to the HSPS system is measured using a current transducer. To reduce the scheme cost, instead of a relay, one IED is installed at the beginning of each feeder. The measurement noises are attenuated by a simple moving average filter (MAF) as [27]

$$i_{\text{feeder}}(kT_s) = \frac{1}{N}\sum_{j=k-N+1}^{k} i_{\text{feeder}}^{\text{meas}}(jT_s), \tag{1}$$

where $i_{\text{feeder}}^{\text{meas}}$ and i_{feeder} are the measured and filtered feeder currents, respectively, and N is the length of MAF window.

The scalability of the proposed method is enhanced by normalising the filtered current i_{feeder} as

$$i_{\text{feeder}}^{\text{pu}}(kT_s) = \frac{i_{\text{feeder}}(kT_s)}{I_{\text{base}}}, \tag{2}$$

where $i_{\text{feeder}}^{\text{pu}}$ and I_{base} are the normalised feeder current and base current, respectively. The latter current is determined based on the nominal power and nominal voltage of the feeder DER. k and T_s are the sampling step and sampling time, respectively.

To address the problem of the low sensitivity of the conventional protection system of the HSPS system, the superposition theorem [28] is used. According to this theory, the current signal consists of normal-running and fault-imposed components. The latter is independent of the former and poses a signature of fault. The superimposed network can be used to calculate the fault-imposed component as

$$i_{\text{feeder,FI}}^{\text{pu}}(kT_s) = i_{\text{feeder,F}}^{\text{pu}}(kT_s) - i_{\text{feeder,N}}^{\text{pu}}(kT_s), \tag{3}$$

where $i_{\text{feeder,FI}}^{\text{pu}}$, $i_{\text{feeder,F}}^{\text{pu}}$, and $i_{\text{feeder,N}}^{\text{pu}}$ are the fault-imposed, fault (during fault), and normal-running (pre-fault) components of the normalised feeder current. A common method to calculate the fault-imposed component is to use the Delta filter [29] as

$$i_{\text{feeder,FI}}^{\text{pu}}(kT_s) = i_{\text{feeder}}^{\text{pu}}(kT_s) - i_{\text{feeder}}^{\text{pu}}(kT_s - T_d), \tag{4}$$

where T_d is the time delay of the Delta filter.

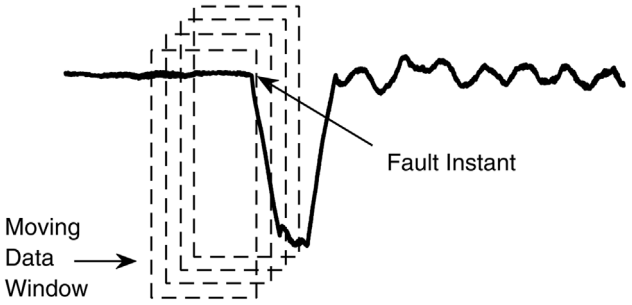

FIGURE 3 Fault-imposed current waveform of a feeder

Due to the DC nature of the current signal, the fault-imposed component is nearly zero (due to the presence of normal disturbances is not exactly zero) during normal conditions while it is non-zero when a fault occurs,as shown in Figure 3. Thus, even a high-resistance fault occurs, the non-zero value of the fault-imposed component can be used as a promising fault detection feature.

3.2 | Stage 2: Forced Helmholtz oscillator

During a high-resistance fault condition, the fault current is not high enough to strongly increase the fault-imposed component. It may result in a malfunction of the fault-imposed current-based protection strategy during normal disturbances. Consequently, to more increase the sensitivity of the proposed scheme, the FHO is employed as follows.

3.2.1 | Operating principle

The second-order differential equation of FHO as an asymmetrical nonlinear oscillator is expressed as [30]

$$\frac{d^2x(\omega_{\text{os}}t)}{d(\omega_{\text{os}}t)^2} + \mu\frac{dx(\omega_{\text{os}}t)}{d(\omega_{\text{os}}t)} + \alpha x(\omega_{\text{os}}t) - \beta x(\omega_{\text{os}}t)^2 = F\sin(\omega_{\text{os}}t), \tag{5}$$

where ω_{os} is the Helmholtz forcing signal frequency. μ and F are the damping level and forcing amplitude, respectively, and α and β are the positive constants. By defining the system output y as [30]

$$y = \frac{dx(\omega_{\text{os}}t)}{d(\omega_{\text{os}}t)} = \frac{1}{\omega_{\text{os}}}\frac{dx(\omega_{\text{os}}t)}{d(t)}, \tag{6}$$

one can write

$$\frac{dy}{dt} = \omega_{\text{os}}\left(-\mu y - \alpha x + \beta x^2 + F\sin(\omega_{\text{os}}t)\right). \tag{7}$$

If F exceeds its critical values F_c, the system state changes from normal motion to the chaotic motion. Indeed, F_c determines the boundary of stable and unstable modes of FHO.

The promising feature of FHO is that by changing the system state to chaotic motion, its output reaches infinity because the system is unstable. By adding small turbulence, the proposed protection scheme is developed that operates based on the condition of the system state during various conditions. During a fault condition, the FHO output is infinity while during normal operation, its output is non-infinity; it facilitates fault detection.

3.2.2 | FHO-based directional element

Using the superimposed component of current, the modified FHO equation is expressed as

$$\frac{d^2x(\omega_{os}t)}{d(\omega_{os}t)^2}+\mu\frac{dx(\omega_{os}t)}{d(\omega_{os}t)}+\alpha x(\omega_{os}t)-\beta x(\omega_{os}t)^2 = F'\sin(\omega_{os}t), \tag{8}$$

where F' is the modified forcing amplitude and is defined as

$$F'=0.5F_c-i^{pu}_{feeder,FI}. \tag{9}$$

The IED of each feeder calculates the output of the modified FHO equation. During the normal operation that the fault-imposed current is zero, $F'=0.5F_c<F_c$ and thus, the system output is in the stable mode. By solving (6) and (7), the maximum value of y during normal conditions is determined equal to 0.60 pu. When a fault occurs, the sign of fault-imposed current determines whether the system motion is normal or chaotic.

Since in an HSPS system, energy storage systems with the bidirectional current flow are available, the pre-fault current in that feeders can be positive or negative. If a DER injects current to the HSPS system, the pre-fault current is positive. When a high-resistance fault occurs in that feeder, the current direction does not change but the current magnitude at the beginning of the feeder decreases. Thus, the fault-imposed component is negative. If a DER is in the charging mode and thus, it absorbs the HSPS energy, the pre-fault current is negative. When a high-resistance fault occurs in that feeder, the current at the beginning of the feeder slightly increases with a negative sign. Therefore, in this case, the fault-imposed component is negative too. It should be noted that for a low-resistance fault, the fault-imposed component is negative in both aforementioned cases. Since the control system of DER units regulates their injected currents, the current of healthy feeders does not change during a fault condition. Thus, the fault-imposed component is nearly zero.

Consequently, for the faulty feeder that $i^{pu}_{feeder,FI}$ is negative, F' becomes greater than F_c and the maximum of system output of modified FHO equation calculated at beginning of the feeder increases to infinity while its peak at healthy feeders is equal to 0.60 pu because $i^{pu}_{feeder,FI}$ is zero and $F'<F_c$. The proposed FHO-based directional element $\mathbb{D}_{FHO}$ is defined as

$$\mathbb{D}_{FHO}=\begin{cases}1, & y=\infty\\ 0, & y<1.\end{cases} \tag{10}$$

If $\mathbb{D}_{FHO}=1$, it interprets as a reverse fault condition and the faulty feeder IED sends the trip signal to its associated solid-state circuit breakers (SSCBs) for isolating this zone from the healthy sections of HSPS, as shown in Figure 1.

To classify the fault condition, the proposed directional element is determined in both positive and negative poles. It should be noted that the absorbed current from the HSPS system is measured in the negative pole. If the directional element in both poles $\mathbb{D}^{+}_{FHO}$ and $\mathbb{D}^{-}_{FHO}$ are 1, the fault is PP. If only one of these directional elements becomes one, the fault is PG.

3.2.3 | Determination of critical forcing amplitude

To determine the boundary of stable and unstable modes of FHO, the Melnikov function $M(t_0)=0$ is solved. To this end, unperturbed homoclinic coordinates (UHCs) are considered in the steady-state. In this condition, the total energy of the system should be zero. Hamiltonian $H(x,y)$ is an operator that in most cases represents the total energy of the system; thus, in the unperturbed steady-state condition, $H(x,y)=0$. The system Hamiltonian is expressed as [30]

$$\begin{cases}dx/dt=\partial H(x,y)/\partial y,\\ dy/dt=-\partial H(x,y)/\partial x.\end{cases} \tag{11}$$

On the other hand, since μ and F are zero in the unperturbed system, (6) and (7) are described in steady-state as [30]

$$\begin{cases}dx/dt=\omega_{os}y,\\ dy/dt=\omega_{os}\left(-\alpha x+\beta x^2\right).\end{cases} \tag{12}$$

To determine the homoclinic coordinates, the following equation can be acquired by substituting (11) in (12) and solving the resulting equation [30]:

$$H(x,y)=\frac{y^2}{2}+\alpha\frac{x^2}{2}-\beta\frac{x^3}{3}=0. \tag{13}$$

The homoclinic orbits q_0^{+} and q_0^{-} are determined by solving (13) for x and y as a function of t as [30]

$$q_0^{+}(t)=\left(+\frac{3\alpha}{2\beta}\sec^2\left(\frac{\sqrt{\alpha}t}{2}\right),\ \pm\frac{3\alpha^{3/2}}{2\beta}\sec^2\left(\frac{\sqrt{\alpha}t}{2}\right)\tan\left(\frac{\sqrt{\alpha}t}{2}\right)\right), \tag{14}$$

$$q_0^-(t) = \left(-\frac{3\alpha}{2\beta}\sec^2\left(\frac{\sqrt{\alpha}t}{2}\right),\right.$$
$$\left.\pm\frac{3\alpha^{3/2}}{2\beta}\sec^2\left(\frac{\sqrt{\alpha}t}{2}\right)\tan\left(\frac{\sqrt{\alpha}t}{2}\right)\right). \quad (15)$$

Thus, the UHCs are expressed as [30]

$$x_0(t) = \pm\frac{3\alpha}{2\beta}\sec^2\left(\frac{\sqrt{\alpha}t}{2}\right),$$
$$y_0(t) = \pm\frac{3\alpha^{3/2}}{2\beta}\sec^2\left(\frac{\sqrt{\alpha}t}{2}\right)\tan\left(\frac{\sqrt{\alpha}t}{2}\right). \quad (16)$$

Using the Melnikov function, one can write [30]

$$M(t_0) = \int_{-\infty}^{+\infty} y(t-t_0)\left(F\sin(\omega_{os}t) - \mu y(t-t_0)\right)dt$$
$$= \int_{-\infty}^{+\infty}\frac{3\alpha^{3/2}}{2\beta}\sec^2\left(\frac{\sqrt{\alpha}(t-t_0)}{2}\right)\tan\left(\frac{\sqrt{\alpha}(t-t_0)}{2}\right)$$
$$\times\left(F\sin(\omega_{os}t) - \mu\frac{3\alpha^{3/2}}{2\beta}\sec^2\left(\frac{\sqrt{\alpha}(t-t_0)}{2}\right)\right.$$
$$\left.\tan\left(\frac{\sqrt{\alpha}(t-t_0)}{2}\right)\right)dt. \quad (17)$$

Solving (17) determines Melnikov function as [30]

$$M(t_0,\alpha,\beta,\delta,F,\omega_{os}) = \frac{6\pi}{\beta}\frac{\omega_{os}^2F\cos(\omega_{os}t_0)}{\sinh\left(\frac{\pi\omega_{os}}{\sqrt{\alpha}}\right)} - \frac{6\mu\alpha^{5/2}}{5\beta^2}. \quad (18)$$

Solving $M = 0$ yields the boundary of stable and unstable modes of FHO [30]. Thus,

$$\frac{6\pi}{\beta}\frac{\omega_{os}^2F\cos(\omega_{os}t_0)}{\sinh\left(\frac{\pi\omega_{os}}{\sqrt{\alpha}}\right)} - \frac{6\mu\alpha^{5/2}}{5\beta^2} = 0$$
$$\Rightarrow \cos(\omega_{os}t_0) = \frac{\mu\alpha^{5/2}\sinh\left(\frac{\pi\omega_{os}}{\sqrt{\alpha}}\right)}{5\pi\beta\omega_{os}^2F}. \quad (19)$$

Since $|\cos(\cdot)|$ is smaller than 1, one can write

$$F \geq \frac{\mu\alpha^{5/2}\sinh\left(\frac{\pi\omega_{os}}{\sqrt{\alpha}}\right)}{5\pi\beta\omega_{os}^2}. \quad (20)$$

If (20) satisfies, FHO enters the unstable mode and its output reaches to infinity. Considering $\alpha = \beta = 1$, the critical value of F as the boundary of stable and unstable modes of FHO is expressed as

$$F_c = \frac{\mu\sinh(\pi\omega_{os})}{5\pi\omega_{os}^2}. \quad (21)$$

Considering $\mu = 0.5$ and $\omega_{os} = 1$ pu, F_c is equal to 0.37. Thus, $F > 0.37$ results in chaotic motion.

3.3 | Flowchart of the proposed algorithm

Figure 4 shows the flowchart of the developed directional protection scheme. In the first stage, the noises of the measured current of each feeder are removed using the MAF. Then, the filtered current signal is normalised and the fault-imposed component of the feeder current is calculated by the IED. In the second stage, the output of the modified FHO equation is calculated by the feeder IED for both positive and negative poles. Based on this output, the proposed directional element is determined. If $\mathbb{D}_{FHO}$ in a feeder becomes one, the feeder is faulty and the IED sends the trip command to the SSCB of that feeder. Based on the values of the proposed directional element in positive and negative poles, the fault type is determined.

3.4 | Practical implementation

IED is a key component of smart systems technology, facilitating the exchange of operational (status points and instantaneous values) and non-operational (waveforms and files) data [31]. According to IEC TS 61850-2, it consists of the processor(s) and can send (receive) data/control to (from) another electronic device such as meters and controllers. The architecture of an IED is shown in Figure 5. It has various functions such as protection, control and logics, metering and power quality analysis, and monitoring [32]. After measuring the analog current signals of both poles, they are converted to digital signals by the A/D converter. The discrete signals are processed and the proposed directional elements are calculated that have binary values of either 0 (no/forward fault) or 1 (reverse fault), based on (10). On the other hand, IED is equipped with a self-monitoring software that this watchdog (WD) service disables all IED functions in the case of an internal error (zero output of WD); WD signal is 1 when IED properly works. According to the logical diagram of the proposed method that is shown in Figure 5, if WD signal is 1 and a fault condition is detected in positive pole, the positive pole circuit breaker (PPCB) signal will be 1 and the trip command is sent to the SSCB of positive pole. Also, in the case of a detected negative pole fault while IED has no internal error, the negative pole circuit breaker (NPCB) signal will be 1. In the case of a detected PP fault, both PPCB and NPCB signals will be 1 provided that WD signal is 1.

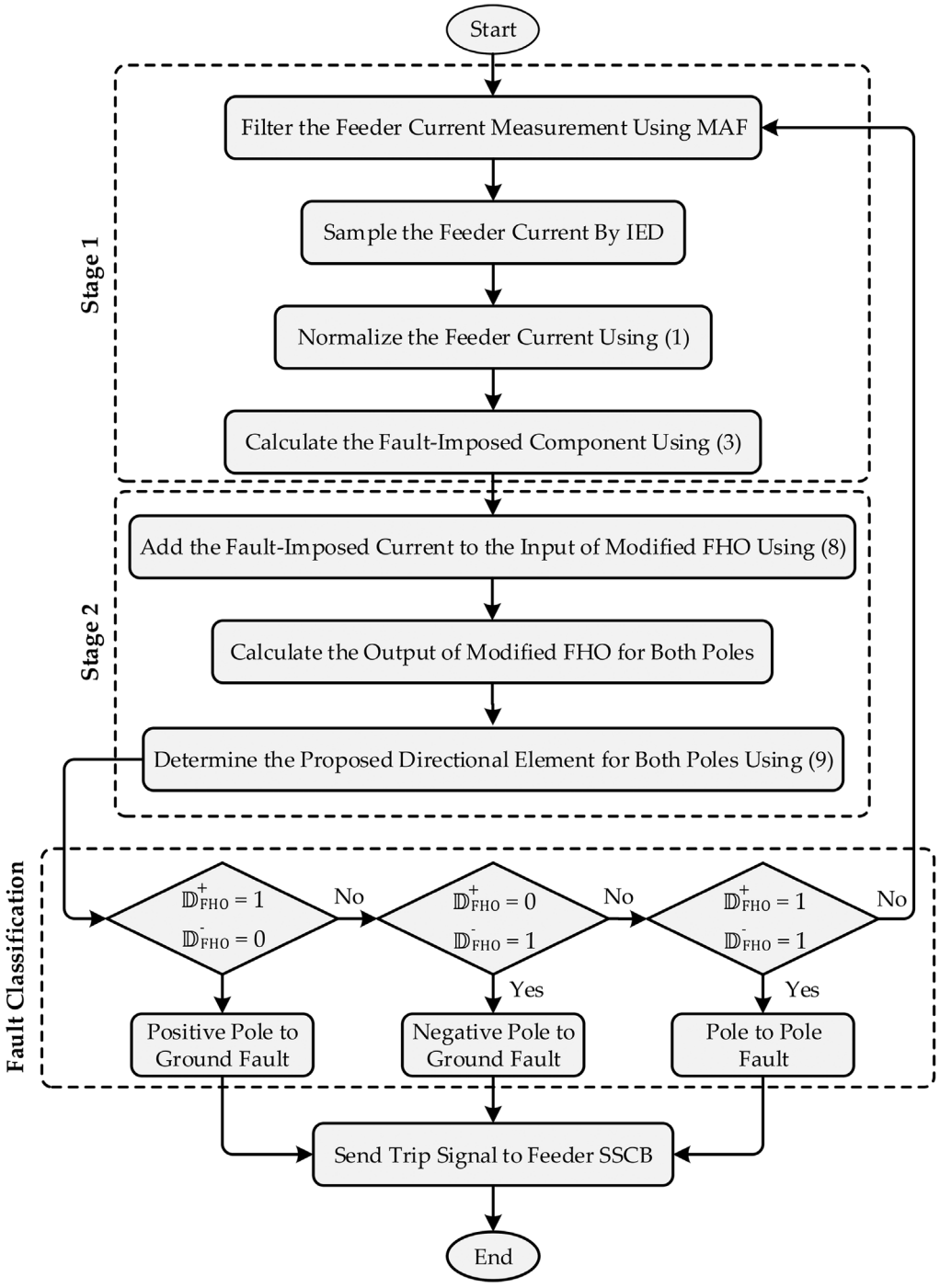

FIGURE 4 Flowchart of the developed FHO-based directional protection strategy

4 | PERFORMANCE EVALUATION

This section is dedicated to evaluating the effectiveness of the proposed protection strategy. To this end, the study HSPS system of Figure 1 is simulated in MATLAB/Simulink environment and several fault conditions are studied. The reference currents of converters of the gas turbine, battery, supercapacitor, and PV is considered equal to 50% of their nominal currents, i.e. 66.67 A, –46.67 A, 20 A, and 46.67 A, respectively. The length of the MAF window, sampling frequency, and the time delay of Delta filter are adopted equal to 300 samples, 5 kHz, and 0.03 s, respectively.

4.1 | Case 1: PG high-resistance fault in unidirectional converter

The first case study is dedicated to investigating the developed protection scheme for a PG high-resistance fault. To this end, a negative pole to ground high-resistance fault with fault

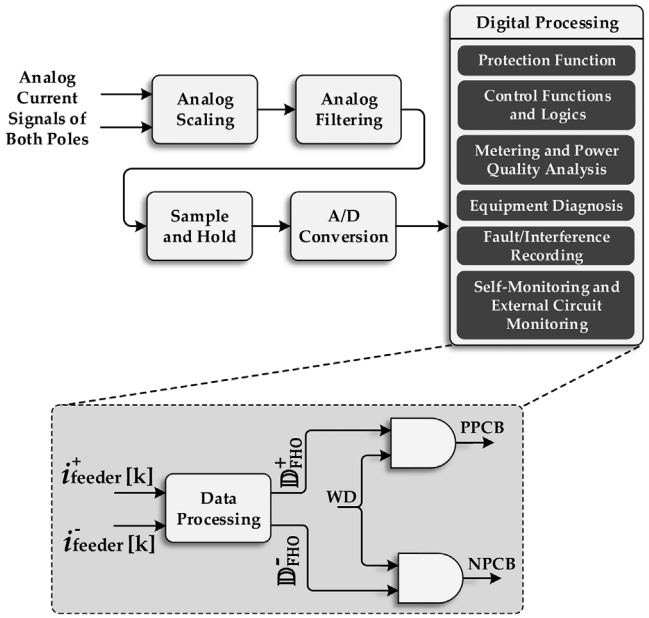

FIGURE 5 Implementation of the proposed method in the IED

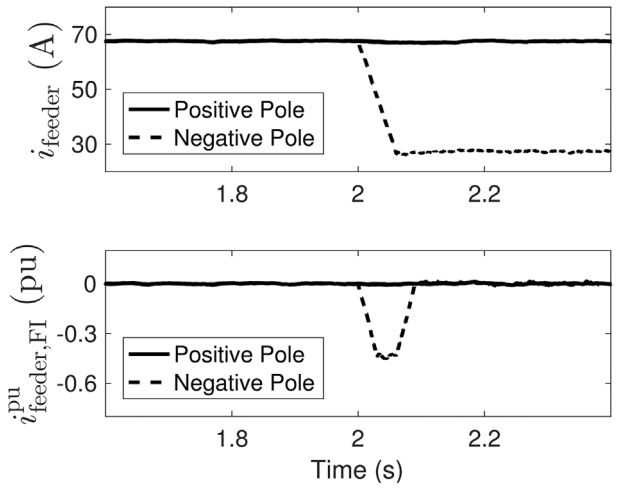

FIGURE 6 Feeder current and its normalised fault-imposed component for a PG high-resistance fault at gas turbine feeder

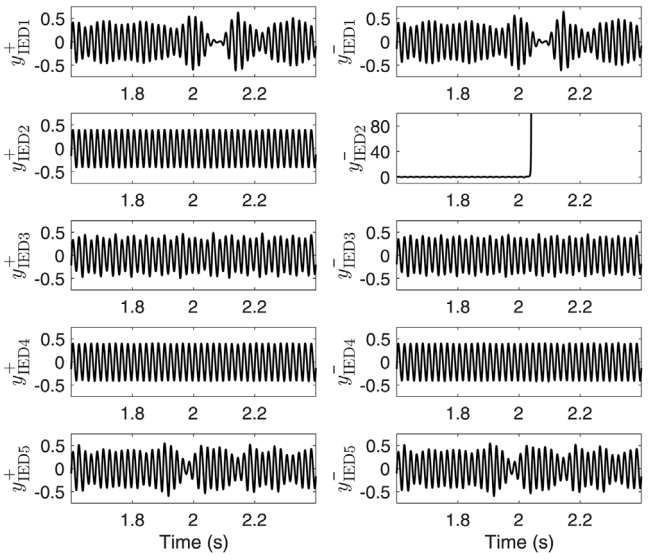

FIGURE 7 FHO output for study HSPS system during a PG high-resistance fault at gas turbine feeder

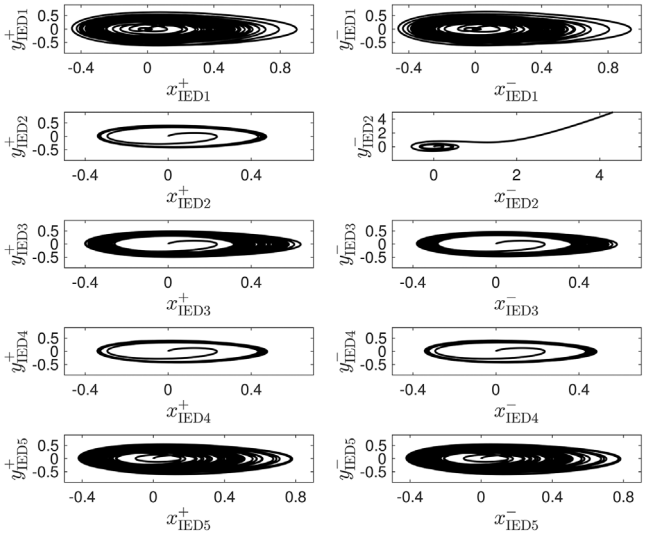

FIGURE 8 Phase portraits of FHO for study HSPS system during a PG high-resistance fault at gas turbine feeder

resistance of 5 Ω is simulated at gas turbine feeder at $t = 2$ s. Figure 6 shows the feeder current and its normalised fault-imposed component during this fault condition. When the fault occurs, the current amplitude reduces from 66.67 to 20.25 A. As the current direction does not change, the conventional protection system of HSPS fails to detect this fault condition. However, the negative value of $i^{pu}_{feeder,FI}$ increases F_c' based on (9), resulting in system becomes unstable. Figure 7 shows the output of the FHO equation calculated by IEDs of HSPS feeders for both positive and negative poles. For the healthy feeders, this output is lower than 1; thus, they are properly interpreted as healthy feeders. However, for the IED of gas turbine feeder (IED2), the FHO output for negative pole is infinity while this output for positive pole is lower than 1. Therefore, IED2 detects a reverse fault and sends the trip command to the associated SSCB. The fault detection time is about 40 ms; this relatively long time for a DC network fault detection does not result in any problem because a high-resistance fault has a limited current amplitude and rate of change, and the fault current is not destructive. Thus, a short fault detection time is not a major priority for a high-resistance fault detection scheme. On the other hand, using advanced routing, the processing delay can be minimised [33] and is in the order of several microseconds that can not affect the performance of the proposed scheme. The fault condition is classified as a negative pole to ground fault. The phase portraits of FHO for all feeders are shown in Figure 8. The system state is the normal motion for all healthy feeders while it is the chaotic motion for the negative pole of IED2.

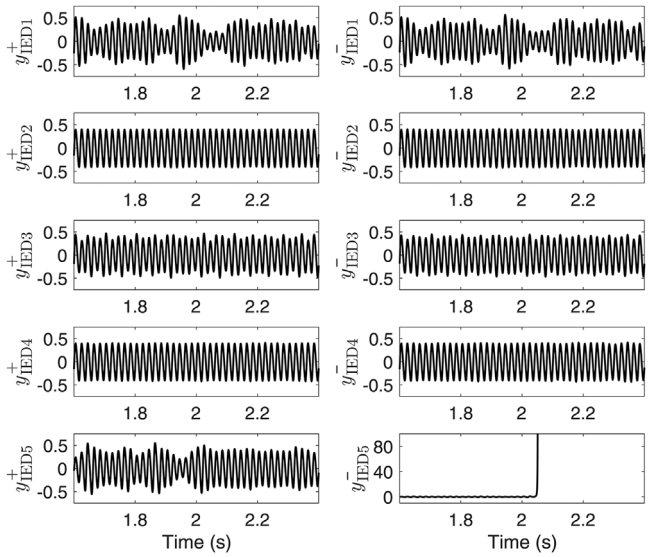

FIGURE 9 FHO output for study HSPS system during a PG high-resistance fault at battery feeder

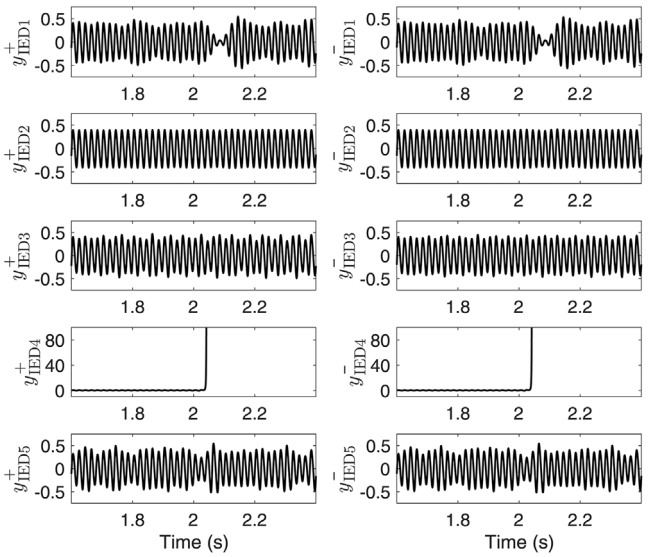

FIGURE 10 FHO output for study HSPS system during a PP high-resistance fault at supercapacitor feeder

4.2 | Case 2: PG High-resistance fault in bidirectional converter feeder

To evaluate the performance of the proposed method in the case of a high-resistance fault in feeders with bidirectional converters, a PG fault (negative pole to ground) is simulated in the battery feeder. Unlike other HSPS sources, battery is in charging mode and the pre-fault current is negative. The fault resistance is 10 Ω and the fault is initiated at $t = 2$ s. The results are shown in Figure 9. The FHO outputs calculated by IEDs of healthy feeders are lower than 1 and the system states are stable in both poles. Also, the system state for positive pole of IED5 is stable while it is unstable in the negative pole of battery feeder and y^-_{IED5} increases to ∞. Thus, $\mathbb{D}^-_{FHO}$ at battery feeder becomes 1. The fault detection time is about 40 ms. It verifies the effectiveness of the developed protection strategy for both unidirectional and bidirectional DC–DC converters.

4.3 | Case 3: PP High-resistance fault

Although the high-resistance faults are usually pole to ground, the objective of this scenario is to evaluate the performance of the developed protection scheme in the case of a PP fault. For this purpose, a PP fault is simulated at the supercapacitor feeder with the fault resistance of 50 Ω. Figure 10 shows the FHO output calculated by IEDs of the study HSPS system. The system states for the healthy feeders are stable and $y_{IED} < 1$. While for both positive and negative poles of supercapacitor feeder, the system states are unstable and y^+_{IED4} and y^-_{IED4} increase to infinity. Thus, the proposed method properly classifies this fault condition as a PP fault. Thus, a reverse fault condition is detected by IED4 and it sends the trip command to the associated SSCB. The fault detection time is about 20 ms.

4.4 | Case 4: Parameter uncertainty

To investigate the effect of parameter uncertainty on the performance of the proposed protection strategy, a PP fault with fault resistance of 20 Ω is simulated at the PV feeder. The uncertainty is considered in solar irradiance, environmental temperature, and feeder impedance. To this end, solar irradiance and temperature are decreased by 50% and 40%, respectively, while the feeder impedances are increased by 15%. The outputs of the FHO equation calculated by the IEDs of HSPS feeders are shown in Figure 11. The maximum of FHO outputs for healthy feeders are below 1 and based on (10), $\mathbb{D}_{FHO} = 0$. However, at $t = 2.03$ s, y_{IED3} in both poles increases to infinity and the fault condition is detected. The results verify that the change of the network parameter does not affect the proper performance of the proposed strategy.

5 | CONCLUSION

The conventional protection system of the HSPS system suffers from ineffectiveness for high-resistance faults, where the fault current direction does not change. This paper has proposed a supplementary directional protection strategy to address this problem. The developed high-resistance fault detection strategy relies on one IED at the beginning of each feeder, sampling the feeder current. By calculating the fault-imposed component of the feeder current, a reverse fault can be discriminated from a forward fault because in the former case, the fault-imposed current is negative while it is zero for the latter case. To increase the sensitivity of the proposed strategy,

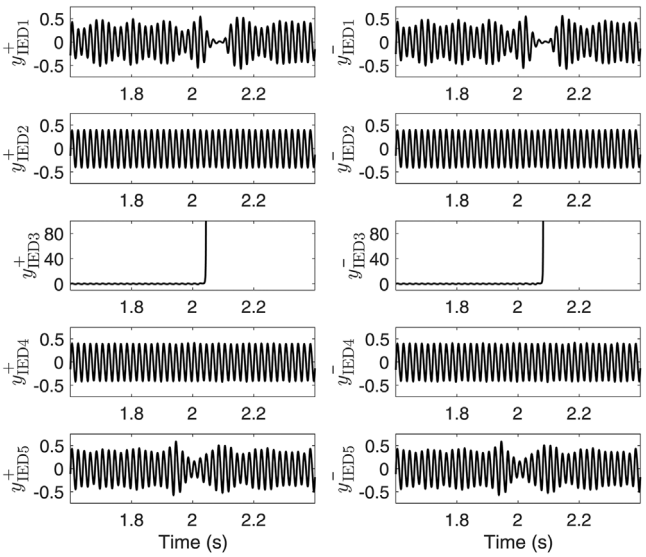

FIGURE 11 FHO output for study HSPS system during a PP high-resistance fault at PV feeder considering parameter uncertainty

the fault-imposed component is added to the FHO equation solved by the feeder IED. The output of the FHO equation is infinity for a reverse fault while it is lower than 1 for a forward fault, facilitating the fault detection. The developed FHO-based protection strategy is local and is effective for both unidirectional and bidirectional converters. Also, it can classify the fault condition. Several case studies on a ±375 V HSPS system verify the effectiveness of the developed protection scheme. Extracting the unique features of high-resistance DC faults for very high-resistance fault detection can be considered as future work.

ACKNOWLEDGEMENT

The authors would like to thank Dr. Bahador Fani for his valuable support.

REFERENCES

1. Xu, D., et al.: Uniform state-of-charge control strategy for plug-and-play electric vehicle in super uninterruptible power system. IEEE Trans. Transp. Electrif. 5(4), 1145–1154 (2019)
2. Li, H., et al.: Fast fault protection based on direction of fault current for the high-surety power-supply system. IEEE Trans. Power Electr. 34(6), 5787–5802 (2019)
3. Li, H., et al.: High-reliability long-backup-time super UPS with multiple energy sources. In: IEEE Energy Conversion Congress and Exposition, IEEE, Piscataway, NJ, pp. 4926–4933 (2013)
4. Shi, K., et al.: Topology of super uninterruptible power supply with multiple energy sources. In: 9th International Conference on Power Electronics and ECCE Asia (ICPE-ECCE Asia). pp. 1742–1749 (2015).
5. Zhou, J., et al.: Control strategy of Li-ion battery module in super UPS. In: International Power Electronics and Application Conference and Exposition, pp. 1236–1241 (2014)
6. Fang, Y., et al.: Fault reconfiguration of super uninterruptible power supply. In: IEEE 8th International Power Electronics and Motion Control Conference (IPEMC-ECCE Asia), IEEE, Piscataway, NJ, pp. 3586–3590 (2016)
7. Han, Y., et al.: Central energy management method for photovoltaic DC micro-grid system based on power tracking control. IET Renew. Power Gener. 11(8), 1138–1147 (2017)
8. Prabhakaran, P., et al.: A novel communication-based average voltage regulation scheme for a droop controlled DC microgrid. IEEE Trans. Smart Grid. 10(2), 1250–1258 (2019)
9. Guerrero, J.M., et al.: Guest editorial: Special section on smart DC distribution systems. IEEE Trans. Smart Grid. 5(5), 2473–2475 (2014)
10. Li, X., et al.: Observer-based DC voltage droop and current feed-forward control of a DC microgrid. IEEE Trans. Smart Grid. 9(5), 5207–5216 (2018)
11. Meghwani, A., et al.: A non-unit protection scheme for DC microgrid based on local measurements. IEEE Trans. Power Delivery 32(1), 172–181 (2017)
12. Meghwani, A., et al.: A new protection scheme for DC microgrid using line current derivative. In: IEEE Power Energy Society General Meeting (2015)
13. Baran, M.E., Mahajan, N.R.: Overcurrent protection on voltage-source-converter-based multiterminal DC distribution systems. IEEE Trans. Power Delivery 22(1), 406–412 (2007)
14. Saleh, K.A., et al.: Hybrid passive-overcurrent relay for detection of faults in low-voltage DC grids. IEEE Trans. Smart Grid. 8(3), 1129–1138 (2017)
15. Yang, J., et al.: Short-circuit and ground fault analyses and location in VSC-based DC network cables. IEEE Trans. Ind.Electron. 59(10), 3827–3837 (2012)
16. Cairoli, P., Dougal, R.A.: Fault detection and isolation in medium-voltage DC microgrids: Coordination between supply power converters and bus contactors. IEEE Trans. Power Electron. 33(5), 4535–4546 (2018)
17. Emhemed, A.A.S., et al.: Validation of fast and selective protection scheme for an LVDC distribution network. IEEE Trans. Power Delivery 32(3), 1432–1440 (2017)
18. Salehi, M., et al.: A poverty severity index-based protection strategy for ring-bus low-voltage DC microgrids. IEEE Trans. Smart Grid. 10(6), 6860–6869 (2019)
19. Mohanty, R., Pradhan, A.K.: Protection of DC and hybrid AC-DC microgrids with ring configuration. In: 7th International Conference on Power Systems, Pune, India (2017)
20. Mohanty, R., Pradhan, A.K.: A superimposed current based unit protection scheme for DC microgrid. IEEE Trans. Smart Grid. 9(4), 3917–3919 (2018)
21. Mohanty, R., Pradhan, A.K.: DC ring bus microgrid protection using the oscillation frequency and transient power. IEEE Syst. J. 13(1), 875–884 (2019)
22. Mohanty, R., Pradhan, A.K.: Protection of smart DC microgrid with ring configuration using parameter estimation approach. IEEE Trans. Smart Grid. 9(6), 6328–6337 (2018)
23. Fletcher, S.D.A., et al.: High-speed differential protection for smart DC distribution systems. IEEE Trans. Smart Grid. 5(5), 2610–2617 (2014)
24. Park, J.D., et al.: DC ring-bus microgrid fault protection and identification of fault location. IEEE Trans. Power Delivery 28(4), 2574–2584 (2013)
25. Dhar, S., Dash, P.K.: Differential current-based fault protection with adaptive threshold for multiple PV-based DC microgrid. IET Renew. Power Gener. 11(6), 778–790 (2017)
26. Dhar, S., et al.: Fault detection and location of photovoltaic based DC microgrid using differential protection strategy. IEEE Trans. Smart Grid. 9(5), 4303–4312 (2018)
27. Peng, W., et al.: Simple carrier recovery approach for RF-pilot-assisted PDM-CO-OFDM systems. J. Lightwave Technol. 31(15), 2555–2564 (2013)
28. Zamani, M.A., et al.: A communication-assisted protection strategy for inverter-based medium-voltage microgrids. IEEE Trans. Smart Grid. 3(4), 2088–2099 (2012)
29. Benmouy, G., Roberts, J.: Superimposed quantities: Their true nature and application in relays, Schweitzer Engineering Laboratories. Inc. Pullman, WA, USA (1999)
30. Bakhshi, M., et al.: Novel islanding detection method for multiple DGs based on forced Helmholtz oscillator. IEEE Trans. Smart Grid. 9(6), 6448–6460 (2018)

31. McDonald, J.D.: Electric Power Substations Engineering. CRC Press, Boca Raton, FL (2003)
32. Lisowiec, A., Nowakowski, A.: Modern ied in today's smart grids. In: International Conference on Clean Electrical Power (ICCEP), pp. 288–292. (2013)
33. Emhemed, A.A.S., et al.: Validation of fast and selective protection scheme for an LVDC distribution network. IEEE Trans. Power Delivery 32(3), 1432–1440 (2017)

How to cite this article: Rouhani R, Sadeghkhani I, Guerrero JM. Directional element for faulty feeder identification of high-resistance fault in high-surety power supply systems. *IET Gener Transm Distrib.* 2021;15:45–55. https://doi.org/10.1049/gtd2.12006